JOURNAL OF SOLID STATE CHEMISTRY 114, 184–189 (1995)

Superstructure Analyses on Single Crystals of $Li_{0.8}VO_2$

Katsuhiro Imai,[1] Hiroshi Sawa, Masayoshi Koike, Masashi Hasegawa, and Humihiko Takei[2]

Institute for Solid State Physics, University of Tokyo, 7-22-1, Roppongi, Minato-ku, Tokyo 106, Japan

Received January 28, 1994; in revised form May 13, 1994; accepted May 18, 1994

Flux-grown single crystals of ordered rock-salt-type $Li_{1-x}VO_2$ ($x \approx 0.2$), which form a significant superstructure in the *ab*-plane and along the *c*-axis at room temperature, have been analyzed by EXAFS and X-ray diffraction methods. The results show that two-dimensionally oriented V ions in the *ab*-plane form a cluster of triangular V_3 trimers with a displacement of 0.160 Å from the unclustered position and that the superstructure along the *c*-axis is due to a stacking order of the V_3 trimers along the *c*-axis. The intensities of the superstructure patterns in X-ray precession photographs are analyzed in terms of the periodic intensity distribution (PID) function, and the most common diffraction streak is caused by a racemate-like stacking sequence of the clustered V layers.

1. INTRODUCTION

The compound $LiVO_2$ has been examined as a key material in the investigation of the unusual magnetic system called "magnetic frustration," because magnetic V^{3+} ions form a two-dimensional triangular lattice (1–5). The crystal structure of $LiVO_2$ consists of Li, V, and O layers stacked along the *[111]* direction of the cubic NaCl lattice with a rhombohedral (pseudohexagonal) symmetry, as illustrated in Fig. 1. Thus, it is said to have ordered rock salt (ORS) structure. In the ideal ORS structure, the V ion lies in the pseudo-hexagonal *ab*-plane with a coordination of six oxygen ions having the same V–O distances, 1.987 Å. Goodenough and co-workers (6, 7) have proposed that all V^{3+} ions in the *ab*-plane of $LiVO_2$ at room temperature are gathered into triangular clusters, called "V_3 trimers," and that the clustering is released above the transition temperature, T_t, of about 500 K.

Recently, our group has successfully synthesized large single-crystal plates of lithium-deficient $Li_{1-x}VO_2$ ($x \approx 0.2$) by the flux method. The characterization and the changes in the structural and physical properties of the crystals have been investigated at temperatures between 4.2 K and room temperature(8). The changes around T_t have also been studied using single-crystal specimens (9).

The as-grown crystals displayed significant superstructure streak patterns along the *c*-axis in single-crystal X-ray diffraction photographs at room temperature (8, 9). The superstructure was found to be a pseudo-hexagonal lattice of $\sqrt{3} \times a_0$ and $2 \times c_0$, suggesting a stacking order of the V_3 trimers along the *c*-axis. However, the precise stacking feature has not been determined as yet.

The present experiments were conducted in order to obtain quantitative results on the formation of V_3 trimers and the exact positions of V ions, as well as to determine the stacking ordering of the V layers using EXAFS and X-ray single-crystal diffraction methods.

2. EXPERIMENTAL

Single-crystal specimens of $Li_{0.8}VO_2$ were prepared by slow cooling from 1100 to 700°C using a flux of the $LiBO_2$–Li_2O system. The details of the growth procedure and the results characterizing the crystal quality have been described elsewhere (8). The as-grown crystals used here were carefully examined in both the X-ray and the electron diffraction intensity distributions, and no indication of asymmetry was observed between the upper and lower parts of the diffraction spots aligned parallel to the *c*-axis. Furthermore, no additional spots without superstructure streaks and spots were found in the X-ray precession photographs of the *ab*-plane. These findings suggest that the crystal specimens have no defect structure except for the superstructure.

EXAFS was carried out using the synchrotron radiation beam at the BL-6B station of the Photon Factory at the National Laboratory for High Energy Physics (KEK), Tsukuba, Japan. Specimens were compressed disks of pulverized crystals mixed with BN powder. The absorption spectra near the vanadium *K*-edge were measured under N_2 gas flow at room temperature and at 573 K using a heating unit. Single-crystal precession photographs were taken using a conventional X-ray source of Mo$K\alpha$ radiation filtered by Zr with a Rigaku Co. Burger precession camera.

[1] Present address: Corporate Research and Development Group, NGK Insulators Ltd., Suda-cho, Mizuho-ku, Nagoya 467, Japan.

[2] To whom correspondence should be addressed.

0022-4596/95 $6.00

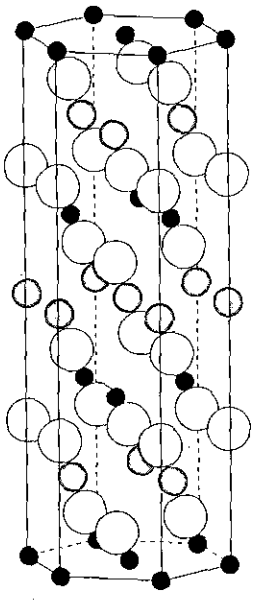

FIG. 1. The average crystal structure of $Li_{0.8}VO_2$ obtained by four-circle X-ray diffractometry (8). The shaded, closed, and open circles indicate Li, V, and O atoms, respectively.

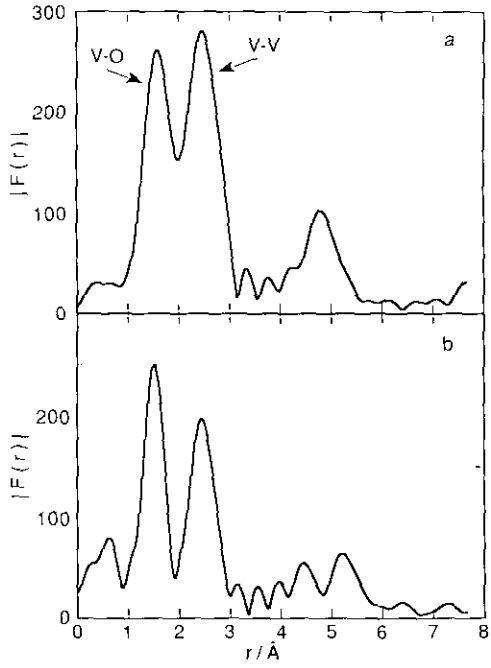

FIG. 2. Fourier transforms of the EXAFS spectra of $Li_{0.8}VO_2$ obtained (a) at room temperature and (b) at 573 K.

3. RESULTS AND DISCUSSION

3.1. Superstructure Analyses in the c-Plane

Figure 2 shows Fourier-transformed patterns of EXAFS spectra measured (a) at room temperature and (b) at 573 K, which is above T_t. Considering the mean atomic distances in single crystals of $Li_{0.8}VO_2$ obtained by the average structure analysis (8), the first and second strong peaks observed in the Fourier-transformed patterns between 1 and 3 Å are uniquely ascribed to those from the first-neighbored V–O and V–V bonds, respectively.

It should be noted that the peaks were broad below T_t but became sharp on heating above T_t. The broadening is due to an overlapping of the separated peaks, and the separation is caused by a displacement of V ions below T_t from symmetric to asymmetric positions in the VO_6 octahedra. Then the six equivalent V–O and V–V distances become inequivalent. ^{51}V NMR studies at room temperature have indicated that all V^{3+} ions lie in a unique environmental situation in the VO_6 octahedra with a lower symmetry than that in the ideal ORS structure (10, 11). These results satisfy Goodenough's V_3 trimer model (6, 7), as schematically shown in Fig. 3, where the displacement occurs in the *c*-plane so as to form a triangle of three V ions. The displacement is also suggested by previous average structure analysis data on single-crystal $Li_{0.8}VO_2$ (8), where V ions have large vibrational factors in the *ab*-plane.

The EXAFS spectra were analyzed with the V_3 trimer model using the least-squares curve fitting method, where two kinds of V–V bonds were assumed, as shown in Fig. 4. Consequently, the values of shorter and longer V–V distances were determined to be 2.562 Å for two V–V bonds and 3.021 Å for four V–V bonds, respectively. The final reliability factor R was 7.9%. Using the obtained distances, the displacement of the V ion from its average position was calculated to be 0.160 Å. This means a shortening of about 6% from the unclustered V–V distance in the sublattice.

In this study, the crystals have about a 20% Li vacancy

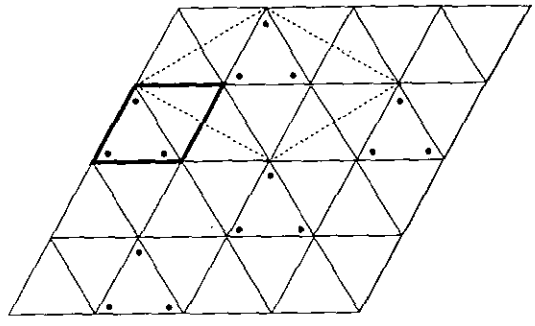

FIG. 3. The V_3-trimer model for the *ab*-plane of $LiVO_2$ proposed by Goodenough and co-workers (6, 7). The dots indicate the positions of displaced V atoms, the thick solid line represents the unit cell of the sublattice, and the thin broken line represents the unit cell of the superstructure.

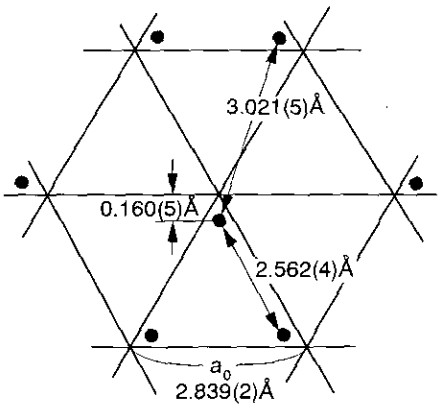

FIG. 4. A schematic drawing of the V_3 trimer. The V–V distances and the displacement of the V ion were determined by EXAFS analysis.

(8). The magnetic measurements have suggested that the Li vacancy induces the equivalent oxidation of the V^{3+} ion to V^{4+}, and the V^{4+} ions are magnetically isolated in the crystal lattice with $S = \frac{1}{2}$ between 4.2 K and room temperature (8). This situation would produce two types of V–V pairs, V^{3+}–V^{3+} and V^{3+}–V^{4+}, and the subsequent EXAFS peak for the V–V bonds would become broader.

The present analysis was performed using the simplified model where the distances of V^{3+}–V^{3+} and V^{3+}–V^{4+} are identical. This model could be justified by the fact that the lattice parameters are not changed much by the Li deficiency between $x = 0$ and 0.2 in $Li_{1-x}VO_2$ (5). Furthermore, the intensity of reflection from the minority V^{3+}–V^{4+} pairs would be quite weak in comparison with those of the V^{3+}–V^{3+} pairs because the number of V^{3+}–V^{4+} pairs is only one-fourth of the V–V pairs in $Li_{0.8}VO_2$. A more detailed EXAFS study using a stoichiometric $LiVO_2$ specimen will give the answer about the exact V^{3+}–V^{3+} distance.

In the present study, however, the V–O distances were not determined by EXAFS because there exist at least four kinds of V–O bonds in the unit cell, and this situation led to difficulties in peak separation. The nearest V–O distances were estimated geometrically by using the lattice parameters and the present V–V data, where three kinds of oxygen ions, O(I), O(II), and O(III), are located at the 6c site of the average structure (8). The obtained V–O values are: three V–O(I) = 1.86 Å, six V–O(II) = 2.06 Å, six V–O(III) = 1.98 Å, and three V–O(III) = 2.12 Å in Fig. 4. The mean V–O value was 2.01 Å, and this value is acceptable for V^{3+}–O^{-2} in the structure of $LiVO_2$.

3.2. *Superstructure Analysis along the c-Axis*

As already reported (8, 9), the precession photographs on the $(h0 \cdot l)$ plane show remarkable superstructure streaks parallel to the c-directions. These patterns have been tentatively explained by a random stacking of the clustered V planes along the c-axis (9). In the present study, however, it has become clear that there exist at least three types of periodicity in the intensity distribution of streak lines witout any change in the fundamental reflections of the sublattice. This is typically shown in the three precession photographs of Fig. 5, in which the lower sections depict schemes of the intensity profiles that are exaggerated for better understanding. The first, A type, represented by Fig. 5a, where the maximum intensity of each streak line periodically appears at $h/3\ 0 \cdot l$ of the sublattice. The second is B type (Fig. 5b), which gives an inverse intensity distribution of A; that is, the minimum intensity is observed at $h/3\ 0 \cdot l$. The final C type represents continuous streak lines, as shown in Fig. 5c. The fact that the sublattice reflections were almost identical in their intensities indicates that the difference can be explained by considering a polytypism in the layer structure.

The present growth experiment showed that the B-type crystals are the most common in comparison with the A- and C-type crystals. The interesting point is that the discontinuous streaks in the A and B types were gradually changed into the continuous ones in the C type by thermal treatments consisting of heating and cooling cycles between room temperature and above t_t.

The continuous intensity distribution observed in the

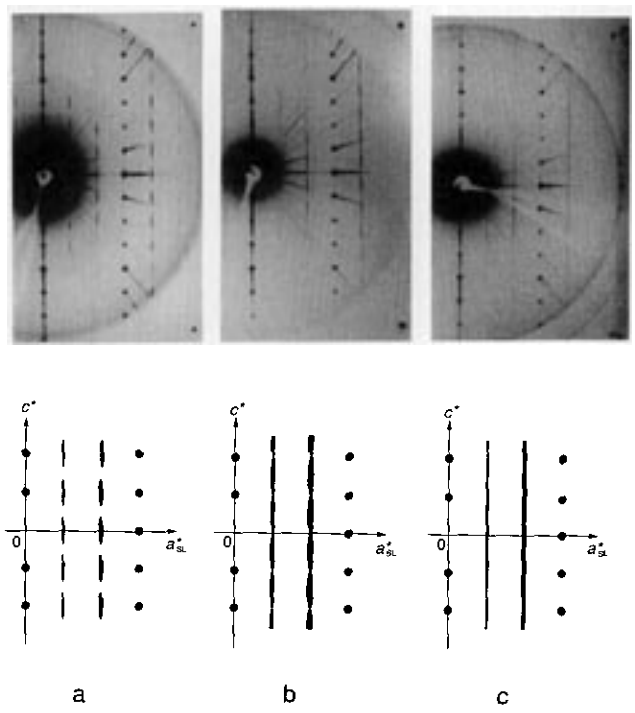

FIG. 5. Three types of superstructure streaks showing the different intensity distributions of X-ray diffraction in the $(h0 \cdot l)$ precession photographs in the upper portion of the figure; the lower portion schematically represents the intensity profiles.

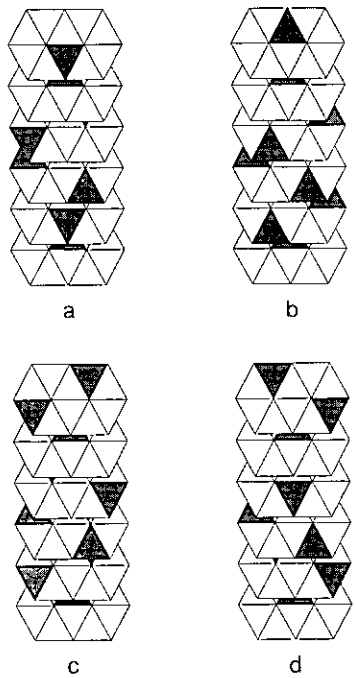

FIG. 6. Schematic drawings for the stacking sequences of the clustered V layers in the *ab*-plane, where only the V layers are illustrated. The hatched triangles represent the V_3 trimers. All stackings are made of six V layers having a 3_1 screw axis with a shift of $1/3a_0$.

C-type crystals is easily explained by considering a complete random stacking of the trimerized V layers along the c-direction, where no interaction for ordering is provided between the V layers. On the other hand, the discontinuous intensity distribution in the A- and B-type crystals can be explained by partially ordered stackings with weak interactions between the V layers, and the difference in the two types of crystals is due to a presumed difference in the stacking of the V layers. The heat treatment would induce a random stacking so as to form the C-type structure.

In order to analyze the superstructure, the intensity distribution was simulated under an implied model of partial ordering in the V layers. As reported previously (8), the X-ray and electron diffraction photographs showed that the length of the c-axis in the superstructure was twice that of c_0 of the sublattice. This means that the ordering should have periodicity $2c_0$. Thus, the model was based on stacking six V layers over the length $2c_0$.

The space group determined from the extinction rule in the precession photographs is $P3_112$ or $P3_212$, which have the screw axis 3_1 or 3_2 along the c-axis. This restriction provides four types of stacking features, as illustrated in Figs. 6a–6d, where each fundamental set of six V layers makes up a stacking unit and possesses a 3_1 screw axis perpendicular to the c-plane. The Li and O layers are eliminated from these figures by considerating that the stacking of these layers is regular along the c-axis as in the average structure (8), and that the intensities of superstructure diffractions are not greatly influenced by such a regular stacking. Furthermore, the X-ray reflections by the Li and O atoms are quite weak in comparison with those of the V atoms.

The periodic intensity distribution (PID) function (12, 13) was applied to the four stacking models in Fig. 6 because this function was most suitable for estimating the intensity distribution of diffraction spots along the stacking axis of the layered materials, such as mica crystals (13). The PID function $S^N(hkl)$ is given for N layers as

$$S^N(hkl) = G^N(hkl)/G_0(hkl), \quad [1]$$

$$= \sum_j^N \exp 2\pi i[h\Delta X_j + k\Delta Y_j + l(j-1)/N], \quad [2]$$

where $G^N(hkl)$ and $G_0(hkl)$ are the Fourier transforms of the polytype and the unit layer, respectively, and ΔX_j and ΔY_j are components of the shift vector for the jth layer.

Figures 7a–7d are the calculated diffraction spots on the $h0\cdot l$ reciprocal plane determined by applying the PID function to the V stacking models illustrated in Figs. 6a–6d, where Fig. 6a corresponds to Fig. 7a and so on. It is apparent that the intensity distribution introduced by the model in Fig. 6a is very close to that of the A type in Fig. 5a. On the other hand, no intensity distribution similar to that for the B type in Fig. 5b was obtained by simulation from the four stacking models in Fig. 6.

It should be noted that the model proposed in Fig. 6d has an enantiomorphous modification with a 3_2 screw axis

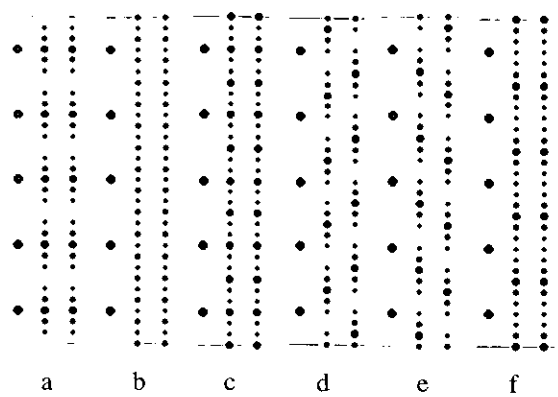

FIG. 7. Illustration of the periodic intensity distribution of $0\ 0\cdot l$, $1\bar{0}\cdot l$, and $2\bar{0}\cdot l$ diffractions with $l = \pm 15$ calculated using the PID function. The results in (a)–(d) were obtained from the ordered-stacking models shown in Figs. 6a–6d, respectively. (e) and (f) were from an enantiomer of the Fig. 6d model and from its racemic modification, respectively.

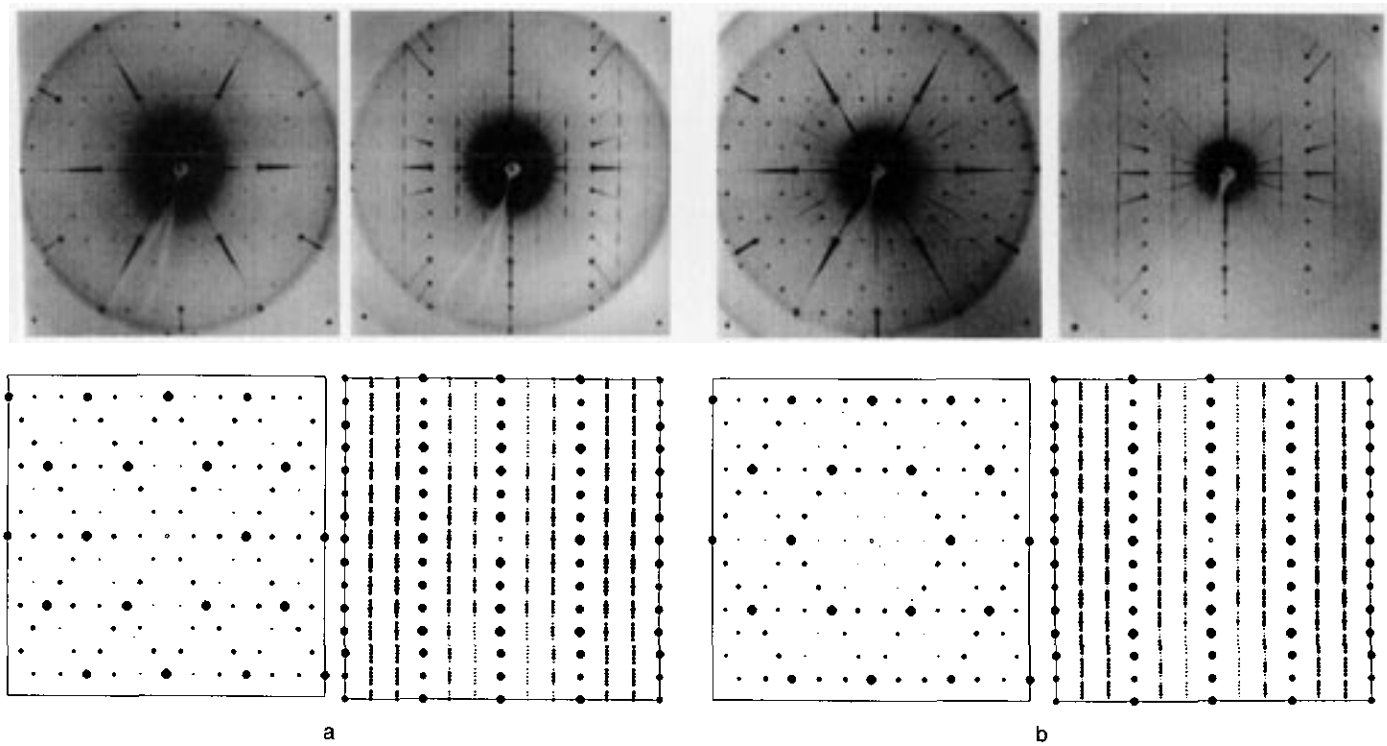

FIG. 8. Observed and simulated intensity profiles of the $h\ k \cdot 0$ (left) and $h\ 0 \cdot l$ (right) X-ray diffractions. The calculated patterns (a) and (b) are obtained using the stacking model of Fig. 6a and the racemic modification of Fig. 6d, respectively, where the logarithmic intensity was proportionally expressed as the diameter of the closed circles.

perpendicular to the c-plane, and the modification gives another intensity distribution, illustrated in Fig. 7e, which is a mirror pattern of Fig. 7d. Using a linear combination of the PID function for Fig. 7d with that of Fig. 7e in equal weights, the intensity profile close to that of the B type was successfully simulated, as shown in Fig. 7f. This success suggests that the B type is a racemiform of the Fig. 6d structure.

The simulated diffraction intensity of the superlattice using the data of all constituent atoms is semiquantitatively represented in Fig. 8, where the diffraction intensity on a logarithmic scale was proportionally expressed as the diameter of each closed circle. The Lorentz correction to the intensities was not applied, and no stacking fault was accounted for in this simulation. Simulation of the A-type diffraction was obtained using the stacking sequences illustrated in Fig. 6a with a 0.160 Å-displacement of V ions, as shown in Fig. 8a. The B-type pattern was also obtained, as shown in Fig. 8b, using the racemiform of the c-axis stacking of the structure shown in Fig. 6d.

The most probable origin of the racemi-like pattern is explained by introducing a twinning structure, where the contact plane is parallel to the ab-plane and where the twinning axis is along the c-axis. Since the simulation of the B-type pattern was successful using an equal combination of the two PID functions, the integrated mass of each twin domain should be almost the same, although the sizes are unclear. Such a twinning structure would decrease the internal energy of the crystal by forming a domain boundary, as in the case of many twinned crystals. Consequently, the evidence that the major portion of as-grown crystals have the B type pattern is reasonably explained by the postulated racemic model. Why the present $Li_{0.8}VO_2$ crystals have three types of superstructure in the V-layer stacking and what kind of interaction correlates each layer remain unanswered.

4. CONCLUSIONS

The precise analyses of the crystal structure of $Li_{0.8}VO_2$ using well-characterized single-crystal specimens grown from $LiBO_2$–Li_2O high-temperature solution have been performed by EXAFS and X-ray precession methods. EXAFS revealed the formation of V_3 trimers at room temperature with a displacement of 0.160 Å from the unclustered V position of the typical ORS structure. The superstructure patterns along the c-axis observed in the X-ray precession photographs were successfully analyzed by applying the PID function to the ordered stackings of the clustered V layers. The most common stacking was

stabilized by a racemate-like ordering in the clustered V layers.

ACKNOWLEDGMENTS

The authors express their sincere thanks to Professor H. Takeda of the University of Tokyo for kind advice on the application of the PID function. They also express their gratitude to Professor I. Nakai of the Science University of Tokyo and his collaborators for their help with the EXAFS experiments. This work was partly supported by the Grant for Scientific Research on Priority Areas "Crystal Growth Mechanism in Atomic Scale" from the Ministry of Education, Science, and Culture, Japan.

REFERENCES

1. P. F. Bongers, Ph.D. Thesis, University of Leiden, Leiden, The Netherlands, 1957.
2. B. Rueter, R. Weber, and J. Jaskowski, *Z. Elektrochem.* **66,** 832 (1962).
3. J. B. Goodenough, *Phys. Rev.* **120,** 67 (1960).
4. T. A. Hewston and B. L. Chamberland, *J. Solid State Chem.* **59,** 168 (1985).
5. A. Manthiram and J. B. Goodenough, *Can. J. Phys.* **65,** 1309 (1987).
6. J. B. Goodenough, "Magnetism and Chemical Bonds," p. 296. Wiley–Interscience, New York, 1963.
7. J. B. Goodenough, G. Gutta, and A. Manthiram, *Phys. Rev. B* **43,** 10170 (1991).
8. H. Takei, M. Koike, K. Imai, H. Sawa, H. Kadowaki, and Y. Iye, *Mater. Res. Bull.* **27,** 555 (1992).
9. K. Imai, M. Koike, H. Sawa, and H. Takei, *J. Solid State Chem.* **102,** 277 (1993).
10. M. Onoda, T. Naka, and H. Hasegawa, *J. Phys. Soc. Jpn.* **60,** 2550 (1991).
11. J. Kikuchi, private communication.
12. R. Sadanaga and H. Takeda, *Mineral. J.* **4,** 159 (1964).
13. H. Takeda, *Acta Crystallogr.* **22,** 845 (1967).